Taylor & Francis
Taylor & Francis Group

Super-compressible and mechanically stable reduced graphene oxide aerogel for wearable functional devices

Keerti Rathi and Duckjong Kim

School of Mechanical and Aerospace Engineering, Gyeongsang National University, Jinju, South Korea

ABSTRACT

The graphene-based aerogels with good electrical conductivity and compressibility have been reported. However, it is challenging to fabricate the graphene aerogel to have excellent mechanical stability for its application in wearable devices. Thus, inspired by macroscale arch-shaped elastic structures and the importance of crosslinking in microstructural stability, we synthesized the mechanically stable reduced graphene oxide aerogels with small elastic modulus by optimizing the reducing agent to make the aligned wrinkled microstructure in which physical crosslinking is dominant. We used L-ascorbic acid, urea, and hydrazine hydrate as reducing agents to synthesize the graphene aerogels rGO-LAA, rGO-Urea, and rGO-HH, respectively. Hydrazine hydrate was found to be best in enhancing the physical and ionic interaction among graphene nanoflakes to achieve a wavy structure with excellent fatigue resistance. Notably, the optimized rGO-HH aerogel maintained structural stability even after 1000 cycles of compression of 50% strain and decompression, showing 98.7% stress retention and 98.1% height retention. We also studied the piezoresistive properties of the rGO-HH aerogel and showed that the rGO-HH-based pressure sensor exhibited excellent sensitivity ($\sim$5.7 kPa^{-1}) with good repeatability. Hence, a super-compressible and mechanically stable piezoresistive material for wearable functional devices was demonstrated by controlling the microstructure and surface chemistry of the reduced graphene oxide aerogel.
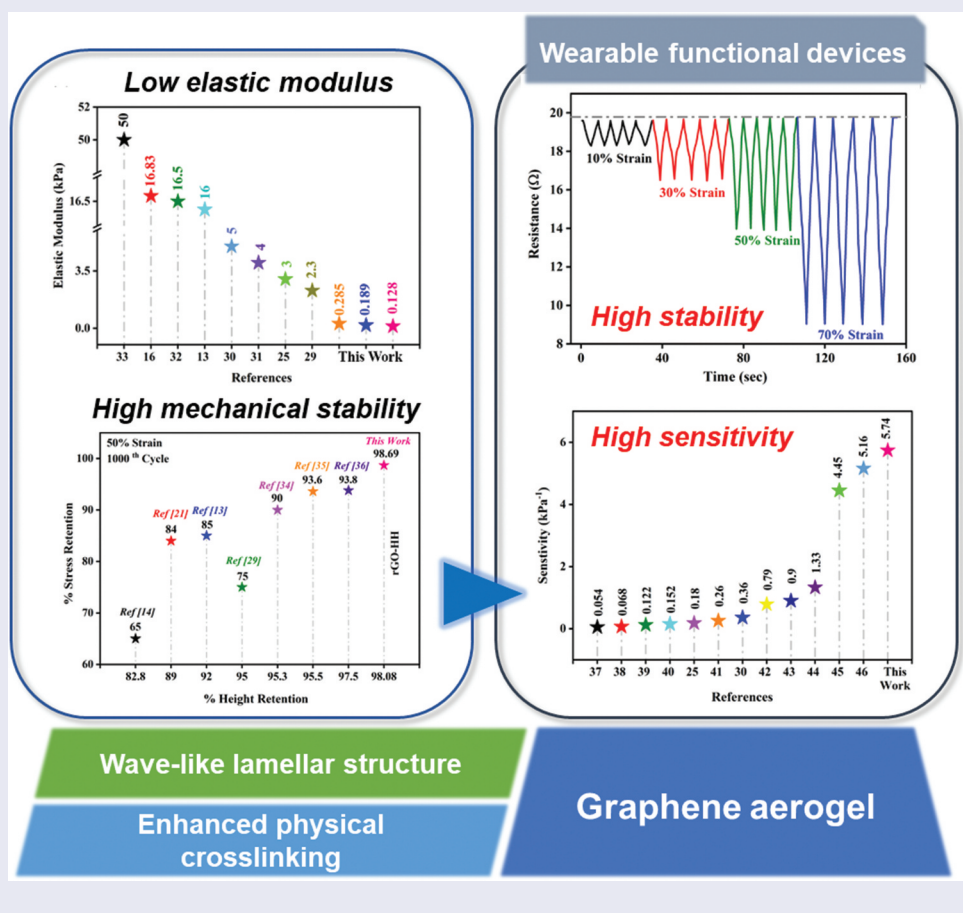
CONTACT Duckjong Kim ✉ dkim@gnu.ac.kr 🏢 School of Mechanical and Aerospace Engineering, Gyeongsang National University, 501, Jinju-daero, Jinju, Gyeongnam 52828, South Korea

1. Introduction

Elastic functional materials with high mechanical stability and compressibility are essential for various applications such as electronic skin [1–3], and wearable devices [4,5]. Recently, conductive aerogels synthesized by active materials such as MXene [2,3], metal-organic frameworks (MOFs) [6], graphene [4,5,7,8], etc. have been used for wearable electronic devices because of their good electrical conductivity and elasticity. MXene aerogel showed good mechanical characteristics. For example, Hu et al. [2] fabricated the MXene aerogel with high compression elasticity and pressure sensitivity. The sensitivity of the pressure sensor was significantly high (~80.41 kPa^{-1}) owing to a low elastic modulus (high compression under less stress). Though, the major drawback of MXene is its low structural stability because, in contrast to graphene, it would degrade extremely fast in the environment. According to the literature, MOFs [6,9,10] are a novel type of porous materials with high crystalline and tunable structure, which have good mechanical properties and a large surface area. However, pure MOFs have been used rarely, owing to the difficulty in shaping and processing the fragile and insoluble MOF crystals. As a result, MOFs have been frequently employed with additives to minimize fragility and enhance crosslinking of the MOF aerogel. Graphene is a promising candidate for conductive aerogels because it has high electrical conductivity due to the two-dimensional SP^2 hybridization structure, allowing electrons to traverse without scattering [11]. Graphene has excellent environmental stability, making them appropriate for industrial applications [12,13]. However, the wearable applications of these conductive aerogels are severely constrained by their poor mechanical stability and high elastic moduli. Typically, conductive materials have high elastic moduli and resistance to elastic deformation, which limits their ability to sense minute pressures. Fabricating supercompressible and mechanically stable with low elastic modulus graphene aerogel is required for wearable device applications.

Several kinds of literature have been published on flexible graphene aerogel in which they tried to enhance the mechanical properties by microstructural modifications. For example, Qiu et al. [14] reported a superelastic cellular structured graphene aerogel produced by freeze drying that retained 76% of its stress and 93% of its height after 1000 cycle tests. Li et al. [15] prepared a macroporous structured Graphene aerogel by a hydrothermal process which showed 96% stress retention after 10 cycling tests under 50% strain. The properly aligned and controllable stacking between the graphene nanoflakes decreases the aggregation during compression, resulting in a mechanically stable aerogel. Also, it has been found that the wavy structure of the graphene aerogel showed more elasticity and mechanical stability because the wave shape behaves like the spring, which increases the recoverability of the aerogel up to the elastic limit [4,16,17]. The structural design, such as lamellar, honeycomb, wavy structure, etc., and the alignment between the nanoflakes are the key attributes to achieving high compressibility, excellent elasticity, and fatigue resistance of the graphene aerogel. The freeze-casting process improves the microstructure of graphene aerogels [4,12,17,18], which offers an ordered and interconnected microstructure [17,19]. For example, Gao et al. [17] fabricated the chitosan-graphene oxide aerogel by bi-directional freezing, which produced the lamellar structure. In accordance with the literature, lamellar structured aerogel demonstrates less strength reduction and plastic deformation than disordered aerogel. It has been found that aligned microstructure is formed through freeze casting, but it is not employed to form proper crosslinking between graphene nanoflakes. So, to create the proper crosslinking during the freeze casting, additives are highly required. The primary role of additives is to make effective crosslinking between the graphene nanoflakes, which helps to improve mechanical stability. The aerogel structure becomes more crosslinked and compact with the addition of additives, which enhances the mechanical strength [5,18,20–24]. For example, Zhang et al. [24] prepared the graphene/cellulose nanocrystal (GCHA) aerogel, which has low density, flexibility, and high moduli. It has been observed that the compression modulus of GCHAs (GCHA50 ~ 60 kPa under 50% strain), which significantly increased with an increase in the loading of CNCs, can be used to control the mechanical strength. Qin et al. [25] showed how the aerogel could be changed into a flexible and elastic aerogel by including a water-soluble Polyimide (PI) precursor in the mechanically fragile rGO aerogel. With the addition of PI, rGO/PI nanocomposite aerogel exhibits a strong interaction between rGO and PI by a chemical modification which enhances the fatigue resistance and elastic modulus. The increased density and crosslinking by the additives can make the aerogel mechanically stable but also mechanically strong and brittle. This could be due to more chemical crosslinking than physical crosslinking between the nanoflakes. It is very difficult to reform the chemical crosslinker (chemical and ionic bonding) without changing any condition (thermal or chemical) [5,16,26–28]. Thus, the high elastic modulus of the aerogel makes it challenging to develop wearable devices (like strain and pressure sensors) based on the composite aerogel because these

applications require high stress to compress or bend the aerogel. Thus, developing a new fabrication process without additives is necessary.

Thus, inspired by macroscale arch-shaped elastic structures and the role of the crosslinking in microstructural stability, we tried to synthesize the mechanically stable reduced graphene oxide aerogel with small elastic modulus by optimizing the reducing agent because reducing agents act as the crosslinker during the reduction and play an essential role in the microstructure control. We aimed to improve mechanical and electrical qualities without using directed freezing, thermal annealing, or any additional additives and polymers. This work investigated the effect of reducing agents on the inter-sheet interaction and shape of the graphene nanoflakes. The selection criteria for reducing agents depend on the pH condition, composition, and reduction strength. Generally, the reducing agents with high pH are strong reducing agents. The key consideration for choosing the reducing agents with different pH values and strength of chemical agents with different compositions are: (i) a low density and wave-shaped microstructure that realizes high compression and (ii) strong physical crosslinking, ensuring mechanical fatigue resistance. Hence, we characterized the microstructure and surface chemistry of the reduced graphene oxide aerogel synthesized using different reducing agents such as L-ascorbic acid, urea, and hydrazine hydrate. This has helped to gain further insight into the surface chemistry – structure relationship to optimize the reduced graphene oxide aerogel fabrication process. The aerogels prepared under different conditions were used for mechanical and feasibility tests for their application in a piezoresistive sensor.

2. Experimental section

2.1 Materials

Graphene oxide suspension (10 mg/ml) was supplied by the Graphene all (South Korea). Hydrazine hydrate, 24–26% in H_2O (RT), L-ascorbic acid (99%), and urea were purchased from Sigma-Aldrich. All the aforementioned analytical chemicals were used to prepare the graphene aerogels.

2.2 Synthesis of rGO aerogel

Reduced graphene oxide aerogels were synthesized using different reducing agents, such as L-ascorbic acid, hydrazine hydrate, and urea, via a hydrothermal process, as shown in Figure 1. Furthermore, L-ascorbic acid, urea, and hydrazine hydrate have a pH of 3.5, 7, and 10.5, respectively. The mass ratio of the reducing agents with graphene oxide was fixed (GO: reducing agent = 1:1) to investigate the pH influence of the reducing agent on the reduced graphene oxide aerogel. The pH of the rGO-LAA, rGO-Urea, and rGO-HH suspensions after the addition of reducing agents was about 2, 4.5, and 9, respectively, as verified by a pH meter (HANNA, HI 8424). Enhancing crosslinking between the rGO flakes is the primary goal of using reducing agents. Furthermore, 100 mL of 10 mg/mL GO aqueous solution was heated to 40°C. After that, a reducing agent was added to the GO solution under continuous stirring. The mixture was poured into the Teflon-lined stainless-steel autoclave. After that, the hydrothermal procedure was performed for 3 h at 160°C.

After cooling the autoclave to room temperature, the hydrogel was rinsed with de-ionized water several times to remove the debris of reducing agents. The
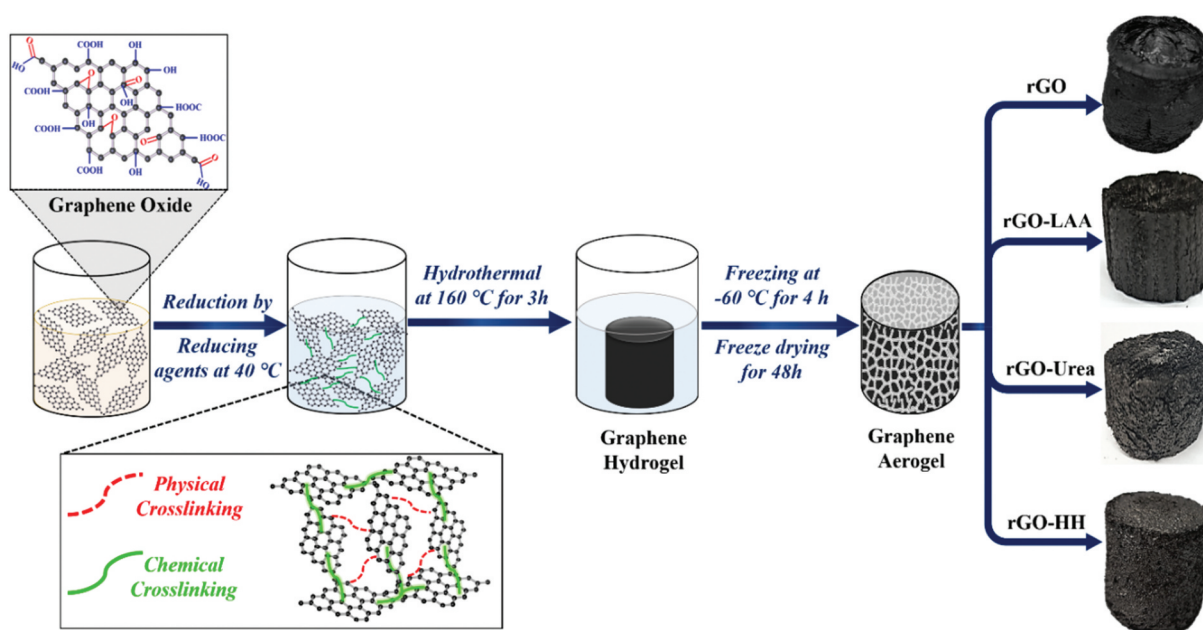

Figure 1. Schematic diagram of the fabrication of rGO aerogels by a hydrothermal process with different reducing agents.

rGO hydrogels produced by different reducing agents (l-ascorbic acid, hydrazine hydrate, and urea) were frozen at −60°C and then freeze-dried for 48 h to form aerogel.

2.3 Characterization

The surface morphology and microstructure of the aerogel were investigated by field emission scanning electron microscopy (FESEM, Tescan S800). Furthermore, hydrogel samples were cut before the freezing process for FESEM analysis owing to their negligible effect on aerogel microstructure. Infrared (IR) spectra of samples were measured using Nicolet iS10 (Thermo Fisher Scientific). X-ray photoelectron spectroscopy (XPS) of reduced graphene oxide aerogels was conducted by NEXSA G2 (Thermo Fisher Scientific). Furthermore, the mechanical compression tests of the aerogels were conducted using JSV-H1000 (Core Tech) at a speed of 150 mm/min. Additionally, three samples were examined for each case of reducing agent to ensure consistency. Moreover, compression experiments were performed five times to test the accuracy of the elastic modulus. The 1000-cycle test at 50% compression strain was used to evaluate the elasticity and mechanical stability of the rGO aerogels: rGO-HH, rGO-Urea, and rGO-LAA. The data acquisition system, DAQ970A (Keysight), was used to measure the electrical resistance of the rGO-HH aerogel while characterizing the piezoresistive properties of the aerogels. The sensor resistance was stabilized for 20 min to obtain a steady baseline resistance. The baseline resistance of the rGO-HH aerogel was 19.7–19.8 Ω.

3. Results and discussion

3.1 Mechanical properties of aerogels

The compression tests for up to 50% strain were conducted for different rGO aerogels to analyze the effect of reducing agents on the stress-strain curve (see Figure 2(a)). We found two regions: a linear elastic region (up to 20% strain) and a densification region (>20% strain) [28]. In the former, stress increased linearly with strain. The slope, in this case, was determined by the crosslinking present in the aerogel [21]. The elastic deformation in this region can be recovered after unloading. In the latter region, the slope of the stress-strain curve increased with strain due to reducing the pores inside the aerogel. The linear-elastic region of rGO-HH was broader (up to 40% strain) than that of the other cases that use reducing agents, which are beneficial for mechanical stability.

Figure 2(b) shows that the linear elastic moduli of the reduced graphene oxide aerogels were significantly small, which is beneficial for developing sensitive piezoresistive pressure sensors. The pH condition can effectively tune the softness of the reduced graphene oxide aerogels during reduction because the elastic modulus of rGO-HH (~0.128 kPa) is smaller than that of rGO-Urea (~0.189 kPa) and rGO-LAA (~0.285 kPa). Our aerogels demonstrated low elastic moduli compared to the other aerogels reported in similar works [13,15,25,29–33] (see Figure 2(c)).

Five cycles of compression-decompression of aerogels were conducted by the mechanical testing machine, as shown in Figure 3(a). Figure 3(b) shows the height recovery for 10–80% strain of the graphene aerogels synthesized with or without reducing agents. Furthermore, rGO-HH showed the best recovery (~92%) at 80% strain, indicating the minimum loss in energy dissipation during the compression-decompression test. In other cases, rGO and rGO-Urea showed approximately ~90% recovery for the same strain. However, in the case of rGO-LAA, the recovery was approximately 90% for 40% strain, which decreased to about 78% for 80% strain.

The stress recoverability also showed mechanical stability because stress retention indicates the amount of the bond structure among the graphene nanoflakes that was recovered after releasing the stress. The cyclic
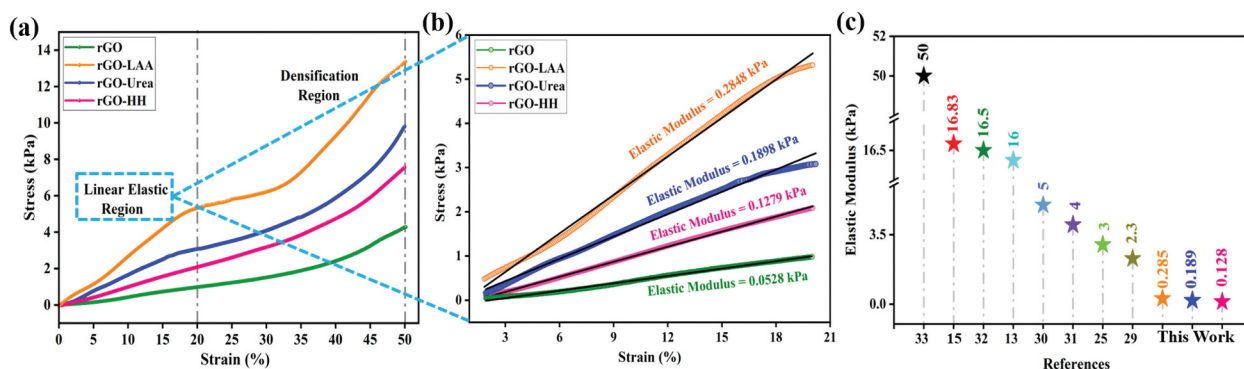

Figure 2. (a) Stress-strain curve for up to 50% strain, (b) Elastic modulus in the linear elastic region, (c) Comparison of elastic modulus of different aerogels in the linear elastic region.
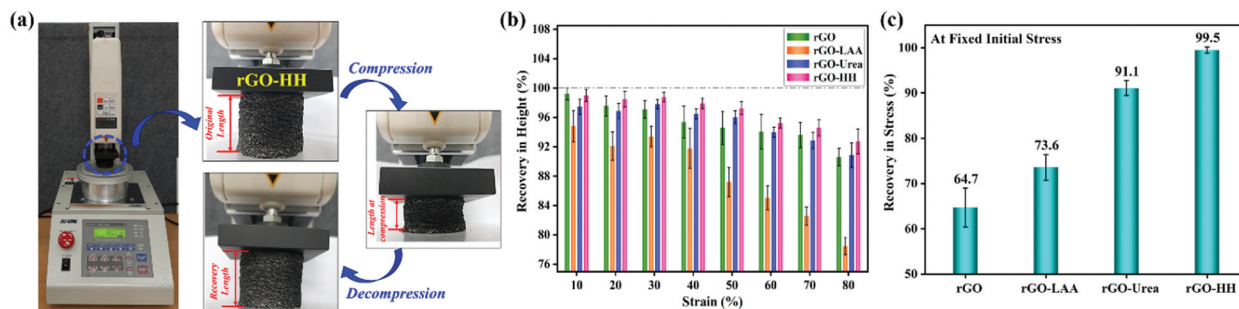
Figure 3. (a) Mechanical testing machine setup, (b) The height recovery test from 10 to 80% strain, (c) The stress recovery test for constant initial stress of rGO, rGO-LAA, rGO-Urea, and rGO-HH aerogels.

test was conducted at constant stress (ranging from 5.68 to 5.96 kPa) to evaluate the stress recoverability of the aerogels, as shown in Figure 3(c). The primary motive for fixing the stress is to observe the change in the elastic modulus by monitoring the strain after the cyclic test. Figure 3(c) shows that the graphene aerogel prepared with or without the reducing agents exhibited a variation in the strain at constant stress because of the different elastic moduli, as explained in Figure 2(b). The recovery of rGO prepared without a reducing agent under stress was ~64.7%, indicating less recoverability of the aerogel. Furthermore, rGO-LAA showed slightly better stress recoverability of ~73.6%. The stress retention of rGO-Urea was ~91.1%, significantly higher than those of the rGO and rGO-LAA. Furthermore, the rGO-HH exhibited near complete recovery under stress (~99.5%) after the 5th cycle, indicating that rGO-HH is the best in fatigue resistance. The fatigue resistance of graphene aerogels can be efficiently controlled by reducing agents having different pH, not just variations in pH conditions, because reducing agents also serve as crosslinking agents. Mechanical test results show that rGO-NaOH aerogel (pH ~ 11) is less mechanically stable than the aerogels prepared with reducing agents (Figure S1). The stress recovery of rGO-NaOH (~66) is slightly greater than that of rGO aerogel (~64.7%), but the height recovery of rGO-NaOH (~71.2%) is much lower than that of rGO (~90%). The lower mechanical stability of rGO-NaOH aerogel confirms that the pH condition is insufficient to guarantee mechanical stability.

Again, to understand the reason behind the mechanical stability, energy dissipation is measured before and after the 20th cycle under 50% strain shown in Figure S2. From the figure, it has been observed that the dissipated energy of aerogels under the same unloading increased in the 1st cycle because of the breakage of the bond and collapse between the graphene flakes. It has been observed that rGO-HH and rGO have low dissipation energy than the rGO-LAA and rGO-Urea. The difference is that the higher the initial cycle amplitude, the greater the energy

releases, particularly when the initial cycle amplitude is larger than the crack initiation threshold. The reason behind the low energy dissipations is less crosslinking, more physical crosslinking, and the wave-shaped structure of the aerogel.

Cyclic tests are needed to confirm the cause of the low energy dissipation. It has been found that the dissipation energy declines with the number of cycles, the crosslinking may rupture in the first cycle, and there will be less bond reformation which is proved in rGO, rGO-LAA, and rGO-Urea. On the other hand, rGO-HH showed significantly less change in dissipation energy after the 20th cycle test, which confirms the reformation of the physical crosslinking after deformation. Therefore, it can be inferred that, under the same unloading stress level, rGO-HH showed little energy dissipation change, meaning there is no further loss in the crosslinking. As a result, we can conclude that at the initial deformation state, the physical crosslinking would play a major role in energy dissipation.

Furthermore, the cyclic test was conducted up to 1000 times under 50% strain to investigate the mechanical stability of the rGO-HH aerogel (see Figure 4(a)). The rGO-HH aerogel showed ~98.7% stress and ~98.1% height retention after the 1000th cycle, significantly higher than the other aerogels tested up to the 20th cycle (Figure S2). However, the height retention of rGO-Urea was approximately similar to that of rGO-HH; its stress retention was ~90.6% at the 20th cycle under 50% strain. Hence, the compression-decompression test was repeated up to the 1000th cycle to examine the mechanical stability of rGO-Urea; moreover, the stress and height retentions of rGO-Urea were reduced to ~38.4% and ~90.8%, respectively (Figure S3).

Hence, rGO-HH demonstrated improved mechanical stability than other aerogels, making it the better choice for wearable device applications.

The stress and height retentions of rGO-HH aerogel after the 1000th cycle under 50% strain is superior to those of other carbon-based materials and their composites, such as PI/rGO/Cobalt [18], Chitosan-FeCl$_3$-CNC [21], GO aerogel [13], biomass-based
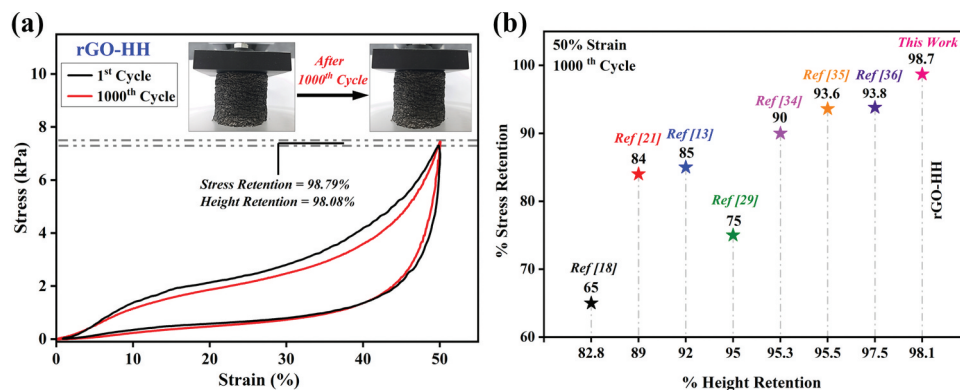
Figure 4. (a) Stress-strain curve of rGO-HH before and after 1000 cyclic test at 50% strain (b) Comparison of height retention and stress retention of different aerogels at 1000th cycle during cyclic test under 50% strain.

carbon aerogel [29], GE/CMC [34], C-CMC/rGO [35], and rGO/CNT-CNF [36] (see Figure 4(b)).

3.2 Mechanism of enhancement in mechanical stability

The IR spectroscopy confirmed the presence of functionalities in the graphene structure, as shown in Figure 5(a). Several types of oxygen functionalities of graphene oxide (GO) were readily identified, namely, edge carboxyl groups (COOH at $1714 \, cm^{-1}$), carbonyls (C-O stretching at 980 and $1067 \, cm^{-1}$), ketone groups (C=O at $1765 \, cm^{-1}$) at vacancy edges, and basal plane hydroxyl and phenol groups (edge hydroxyls) (C – OH at $1341 \, cm^{-1}$) [5]. The vibrational C-H stretching occurred at $2778–3099 \, cm^{-1}$. The presence of physisorbed water was observed on GO surfaces through OH stretching peaks at $3498–3925 \, cm^{-1}$. Moreover, IR spectroscopy of graphene oxide confirmed the presence of oxygen groups and the location of the functionalities (Figure S4(a)).

Some functional groups began to be removed as hydrothermal treatment proceeded without reducing agents, verified by the reduction of O-H and C=O stretching peaks [24]. The C-H stretching peaks ($2861–2957 \, cm^{-1}$) blue shifted when the bond strength increased, as shown in Figure 5(a). However, The C-C stretching peak at $1525 \, cm^{-1}$ indicates that the oxygenated surface groups were significantly removed due to hydrothermal treatment. Therefore, the hydrothermal treatment without reducing agents helps to remove the oxygenated functional groups from the graphene oxide. However, the carboxylic groups ($1708 \, cm^{-1}$) are still on the edge of the aromatic structure. In the opposite case, rGO-NaOH (~pH 11) without a reducing agent showed COOH peak vanished, possibly due to the deprotonation of COOH at high pH. High pH was ineffective in crosslinking between the graphene nanoflakes, as confirmed by the reduction in the peak intensity of

C-H and C-O stretching peaks in IR spectra shown in Figure S4(b).

The peak shifting and generation of the functional groups and binding affinity were studied by IR spectroscopy to investigate the effect of reducing agents on graphene oxide. In the case of rGO-LAA, rGO-Urea, and rGO-HH, reducing agents were selected based on variation in pH from 3.5 to 10.5 because pH is attributed to the altered hydrogen and ionic bonding patterns upon protonation or deprotonation during GO reduction, which was already confirmed by Enrique García-Bordejé et al. [16]. However, pH variation does not enhance the physical and chemical bonding while reducing agents to act as crosslinking agents. This is confirmed by the IR analysis of rGO-NaOH (~ pH 11) without a reducing agent.

IR spectra showed more CH-stretching peaks in the case of rGO-LAA compared to rGO-Urea and rGO-HH. These groups could not form hydrogen bonds; they do not interact with polar compounds like water. Hence, rGO-LAA aerogel has the highest chemical crosslinking. However, The N-H peak at $3315 \, cm^{-1}$ was present in the case of rGO-HH and rGO-Urea because the hydrazine hydrate and urea have the amine structure [29], which enhances the hydrogen bonding. rGO-HH showed another noticeable peak at $1254 \, cm^{-1}$, indicating the presence of C-N stretching. More physical crosslinking occurred because the C-N stretching is polarized toward the nitrogen. However, the same was not found in the case of rGO-Urea. Thus rGO-HH showed high physical crosslinking.

Interestingly, the carboxylic peak ($1708 \, cm^{-1}$) retained its presence in rGO-LAA and rGO-Urea. However, the carboxylic peak vanished in the case of rGO-HH (Figure 5(a)) due to the reduction of GO at high pH because carboxyl groups can be protonated (R-COOH) or deprotonated (R- COO) depending on the pH of the solution [19]. Therefore, the removal of carbonyl/carboxylic groups is favored at high pH values (~9 and 11), which may be due to the ionization
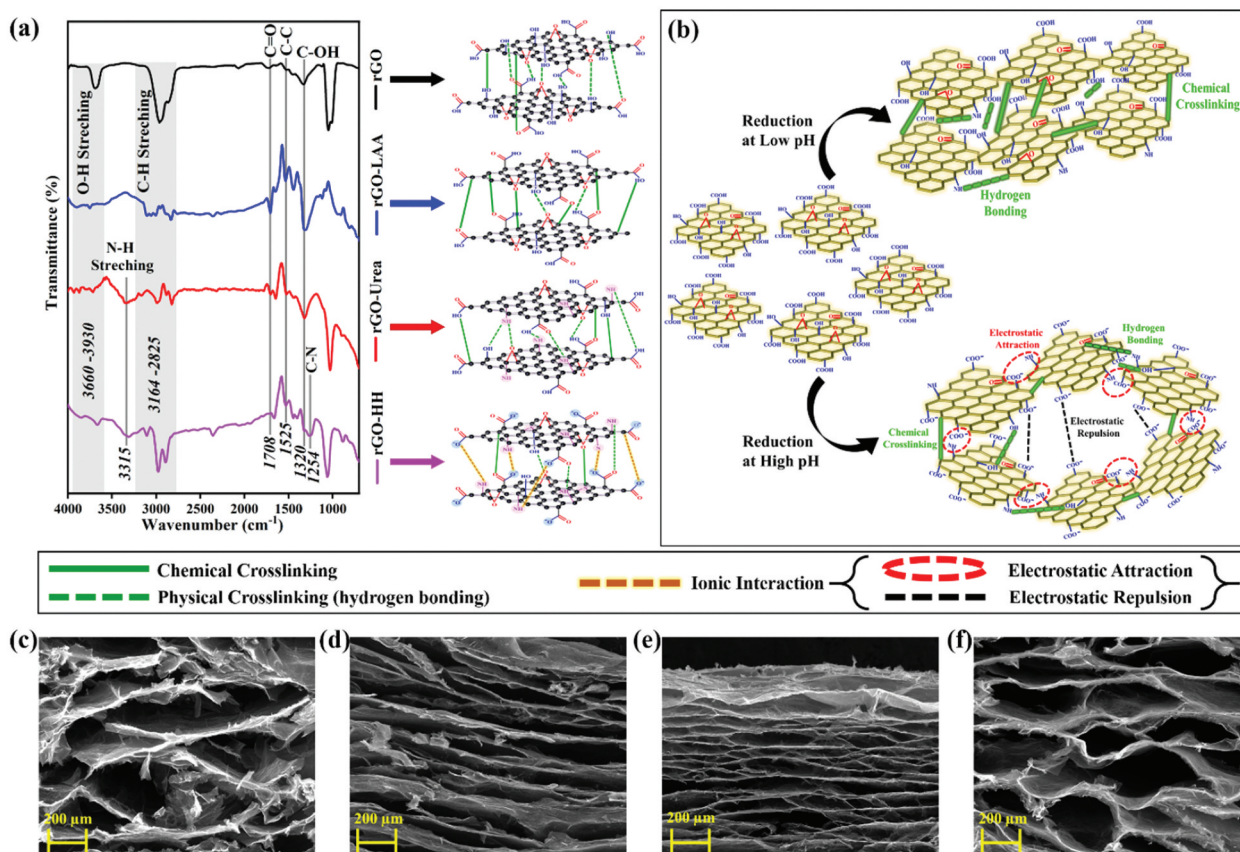
Figure 5. (a) IR spectra of rGO, rGO-LAA, rGO-Urea, and rGO-HH aerogels. (b) Effect of pH condition during the reduction process on the aerogel microstructure. The red dashed line, black dashed line, green dashed line, and bold green line indicate electrostatic attraction, electrostatic repulsion, hydrogen bonding, and chemical crosslinking, respectively. FESEM images of (c) rGO, (d) rGO-LAA, (e) rGO-Urea, and (f) rGO-HH.

of the carboxylic group owing to removing the hydrogen atom as a free proton (H^+) which is confirmed by the XPS analysis (see Figure S5, Tables S1 and S2). Figure S5 demonstrates XPS for comparing the relative proportion of the components derived from the fitting of the O 1s band and C1s band, with the most significant feature being the decrease of the C-O-C band in the O1s peak and the COOH band in the C1s peak by increasing the pH value, which can be attributed to the removal of epoxide and carboxylic groups. The COO negative charge ions were formed on the graphene's edge, known as deprotonated states [14]. The deprotonated states can form ionic interactions with other compounds, creating electrostatic repulsion and attraction (see Figure 5(b)). Table 1 summarizes the effect of reducing agents with varying pH conditions to understand better crosslinking between graphene flakes.

The influence of reducing agents on the structure of the graphene nanoflakes was investigated by FESEM. rGO aerogel without reducing agent contained disordered and discontinuous fragments (see Figure 5(c)), likely due to insufficient crosslinking between the graphene flakes. In the case of rGO-LAA, the gap between the graphene flakes was reduced due to the strong chemical crosslinking, enhancing the aerogel's elastic modulus and compression strength. The morphology of the rGO-LAA was flat lamellar; moreover, it was properly aligned, which may be owing to the increased chemical crosslinking and negligible hydrogen and ionic bonding (see Figure 5(d)).

The structure of rGO-Urea was aligned; however, it was less wavy. Also, it had less space between the graphene flakes, as shown in Figure 5(e). This effect may be attributed to more hydrogen bonding and little ionic interaction. The structure of the rGO-HH was wavier and aligned because of the basicity of hydrazine hydrate (see Figure 5(f)). During the hydrothermal process, the mixture of hydrazine hydrate and GO developed strong physical crosslinking via ionic interaction and hydrogen bonding among the graphene layer. The generated hydrogen bonding and ionic interaction created the electrostatic repulsion-attraction with the π-π and hydrogen bond, which might have crumpled the lamellar structures into wave-shaped lamellar structures during the hydrothermal process. rGO-HH had a low elastic modulus and a higher linear elastic region than rGO-LAA and rGO-Urea because of its wave-shaped structure and more physical crosslinking between the graphene flakes.
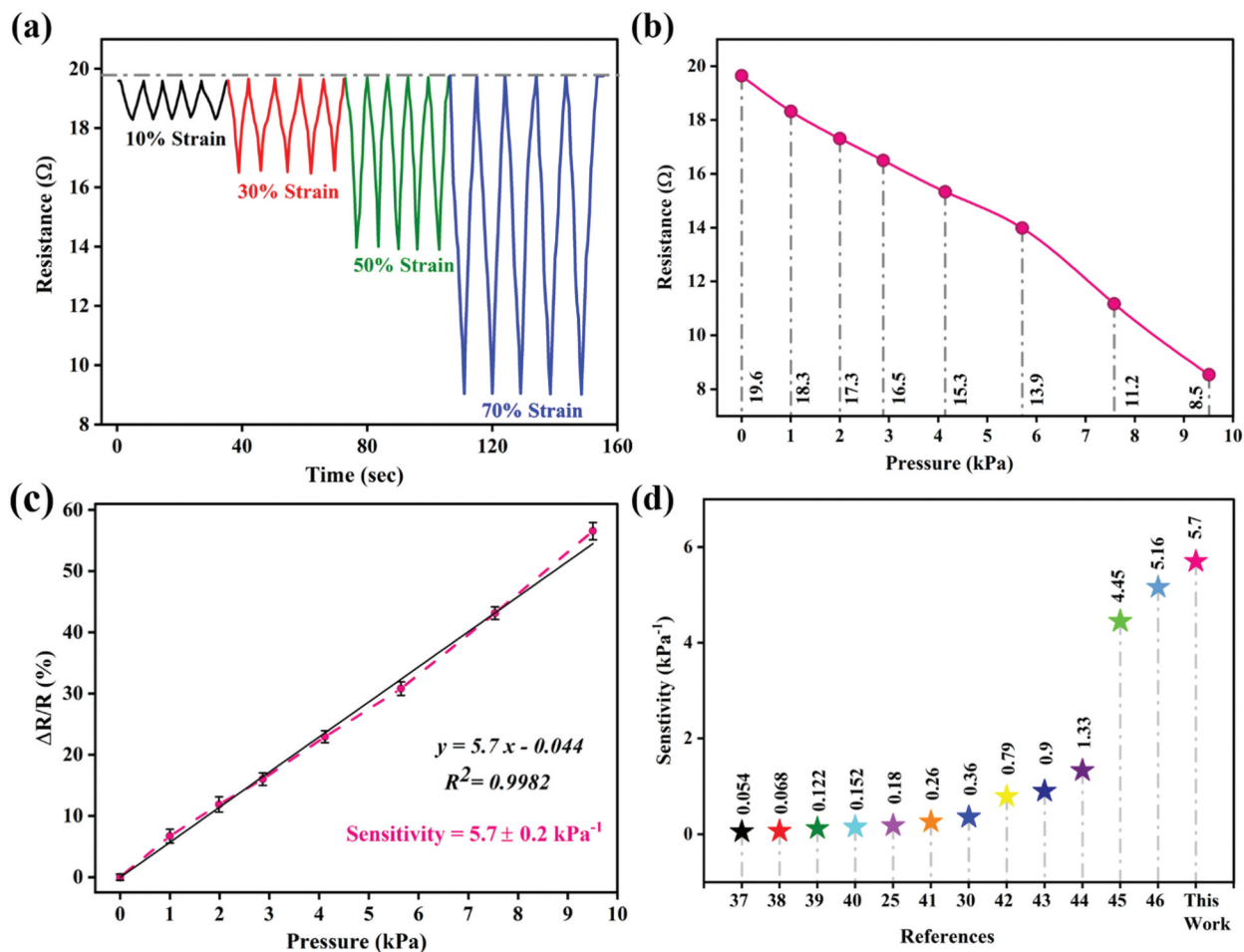
Table 1. Summary of the effect of reducing agent on crosslinking between the graphene nanoflakes.

		rGO	rGO-LAA	rGO-Urea	rGO-HH
C–H Bond (2825–3164 cm^{-1})		◯	⬆◯	⬆◯	◯
N–H Bond (3315 cm^{-1})		✕	✕	◯	◯
C–N Bond (1254 cm^{-1})		✕	✕	✕	◯
C=O Bond (Carboxylic Groups, 1708 cm^{-1})		◯	◯	◯	✕
Change in (compared with rGO)	Chemical crosslinking	—	↑	↑	—
	Physical crosslinking	—	—	↑	⬆
	Ionic interaction	—	—	—	↑

◯ Presence of the bond　　　　　　　⬆◯ Increased number of bonds

✕ No bond　　　　　　　↑ Increased in crosslinking

The energy-dispersive spectroscopy (EDS) mapping was used to confirm the presence of atoms in the graphene aerogel (Figure S6). Carbon and oxygen elements were detected in rGO and rGO-LAA. However, EDS of rGO-Urea and rGO-HH revealed that carbon and oxygen elements appeared with the nitrogen, indicating that graphene flakes were also connected to the nitrogen and contributed to the create physical crosslinking.

We propose the elasticity and stability mechanisms of graphene aerogels based on graphene shape and physical crosslinking between them. Without a reducing agent, graphene nanoflakes are bonded through weak interaction. Hence, rGO fragments are subject to irreversible movement and accumulation when subjected to an external force, reducing their resiliency. The reduction of GO with LAA and urea resulted in strong chemical interaction and a weak physical crosslinking among rGO nanosheets, resulting in rGO-LAA and rGO-Urea with modest layer thickness and spacing in an ordered lamellar structure. The layer gap became narrower and collapsed with each other under extreme compression. The lamellar layer structure did not entirely recover after releasing the stress because the chemical bond reformation was challenging without any conditions (such as temperature or chemicals). Unlike rGO-LAA and rGO-Urea, rGO-HH had a wavy structure like a supporting springboard [17] with high physical crosslinking, contributing to the flexibility of the aerogel. The graphene layer spacing decreased with negligible plastic deformation when stress was applied. After removing the stress, the aerogel rebounded quickly like a springboard. The wave-like lamellar structure and physical crosslinking [30] facilitated rapid crosslink reformation even after releasing the high compressive strain, resulting in fast restoration of the rGO-HH aerogel to its original shape. Combining these properties resulted in a stable structure with high compressibility and elasticity. Hence, the structure should be wavy with physical crosslinking between the graphene nanoflakes for highly mechanically stable and super-compressible aerogel.

3.3. Piezoresistive characteristics of rGO-HH aerogel

The rGO-HH aerogel is a promising candidate for piezoresistive devices owing to its high mechanical stability, super-compressibility, elasticity, and good electrical conductivity. A simple piezoresistive pressure sensor was fabricated by sandwiching the rGO-HH aerogel between two tapes of aluminum joined together by silver paste to study the piezoresistive property of the aerogel (Figure S7). Figure 6(a) shows the real-time resistance variation of the rGO-HH at various compression strains (10–70% strain). The resistance decreased during compression and quickly increased during decompression because the contact area between the graphene flakes influences the conductivity of the rGO-HH aerogel. The contact area among the graphene layers increased during the compression, causing a decrease in resistance (see Figure 6(b)). The cyclic test was conducted up to five times under different compression strains (10, 30, 50, and 70%) to evaluate the repeatability of the resistance caused by the compression, as shown in Figure 6(a). We observed that resistance recovered completely after the 5th cycle, indicating that the rGO-HH aerogel can acts as a stable pressure sensor.

A correlation graph between the percentage response ($\Delta R/R_a\%$) of the sensor versus applied pressures (0 to 9.5 kPa) was plotted to determine the

Figure 6. Piezoresistive response of rGO-HH aerogel. (a) Real-time resistance at different compression strains. (b) Resistance changes at a pressure ranging from 1 kPa to 9.5 kPa. (c) Ultrahigh linear sensitivity in a wide pressure range of 0–9.5 kPa. (d) Comparison of the sensitivity of rGO-HH with other carbon-based sensing materials.

sensitivity (S) of the rGO-HH pressure sensor (see Figure 6c). Mathematically, the sensitivity is defined as [5]

$$S = \frac{\Delta R / R_0}{\Delta P}$$

where ΔR denotes the change in resistance under pressure, R_0 represents the initial resistance before the applied pressure, and ΔP corresponds to the variation in the applied pressure. We observed from the graph based on the least-square method that the linear fitting curve of the rGO-HH sensor at different pressure is represented by y = 5.7× − 0.044, R^2 = 0.9982, where y is the piezoresistive response, x denotes the applied pressure, R^2 is the correlation coefficient. The value of R^2 was 0.9982 (>0.9), indicating that the rGO-HH pressure sensor has good linearity. The rGO-HH had a linear sensitivity of 5.7 ± 0.2 kPa^{-1} under the pressure range of 0–9.5 kPa, demonstrating the wide working range (see Figure 6(c)). The detection limit is a theoretical calculation to estimate the measuring limit of the sensor. It is calculated by dividing the slope of the linear portion of the calibration curve by three times the standard deviation of the initial resistance of the aerogel in the absence

of any pressure. The detection limit of the rGO-HH aerogel-based pressure sensor was approximately 0.0055 kPa. Our sensor demonstrated good performance compared to the sensitivity of other pressure sensors reported in similar works [25,30,37–46] (see Figure 6(d) and Table S3).

The outstanding sensitivity of rGO-HH can be ascribed to (i) the highly compressible and elastic behavior with high mechanical stability and (ii) the wavy structure creating a proportional increase in the contact area and decrease in resistance under compression. These results indicate that our rGO-HH aerogel has high fatigue resistance by excellent structural stability, enabling stable sensing performance.

4. Conclusion

We successfully fabricated the reduced graphene oxide aerogels using different reducing agents (L-ascorbic acid, urea, and hydrazine hydrate) that showed remarkable changes in the surface chemistry and morphology of the graphene nanosheets. The properties of the reduced graphene oxide aerogel were changed based on the reducing agents at different pH values.

We found that the pH affected the surface chemistry of the graphene structure, significantly affecting the microstructure of the graphene aerogel. The morphology of the rGO-LAA (pH ~ 2) and rGO-Urea (pH ~ 4.5) aerogels was lamellar due to the stacking via hydrogen and covalent bonding between the graphene sheets. However, the morphology of the rGO-HH (pH ~ 9) was wave-like, created by the ionic interaction and hydrogen bonding among the graphene nanoflakes. The aligned wave-like structure can effectively transfer stress under large deformation without structural damage, ensuring good shape stability.

On the contrary, the lamellar structure showed good stability at low stress until the friction between the graphene sheets was developed. The rGO-HH aerogel showed super-compressibility (elastic modulus of 0.128 kPa), elasticity, and excellent mechanical stability (98.7% stress retention, 98.1% height retention after the 1000th cyclic test under 50% strain). These enhanced mechanical properties are due to the wave shape microstructure and the strong physical crosslinking among the graphene layers. The excellent mechanical stability and robust microstructure of rGO-HH aerogel are beneficial for piezoresistive performance, resulting in high sensitivity (5.7 kPa^{-1}) and low detection limit (~0.0055 kPa). The excellent mechanical and piezoresistive properties can make the aerogel an attractive candidate for wearable functional devices. We expect our strategy will provide a fascinating way to create new two-dimensional nanomaterial-based aerogels.

Acknowledgments

Disclosure statement

No potential conflict of interest was reported by the author(s).

Funding

Author contributions

Keerti Rathi has done material synthesis, characterization, mechanical testing, and pressure sensing application. Duckjong Kim has contributed to checking the data and analyzing the results. All authors have approved the final version of the manuscript.

ORCID

Duckjong Kim http://orcid.org/0000-0001-6372-8785

References

[1] Yue Z, Zhu Y, Xia J, et al. Sponge graphene aerogel pressure sensors with an extremely wide operation range for human recognition and motion detection. ACS Appl Electron Mater. 2021;3:1301–1310.

[2] Hu Y, Zhuo H, Luo Q, et al. Biomass polymer-assisted fabrication of aerogels from MXenes with ultrahigh compression elasticity and pressure sensitivity. J Mater Chem A Mater. 2019;7:10273–10281.

[3] Zhang S, Tu T, Li T, et al. 3D MXene/PEDOT: PSS composite aerogel with a controllable patterning property for highly sensitive wearable physical monitoring and robotic tactile sensing. ACS Appl Mater Interfaces. 2022;14:23877–23887.

[4] Zhuo H, Hu Y, Tong X, et al. A supercompressible, elastic, and bendable carbon aerogel with ultrasensitive detection limits for compression strain, pressure, and bending angle. Adv Mater. 2018;30:1706705.

[5] Wei S, Qiu X, An J, et al. Highly sensitive, flexible, green synthesized graphene/biomass aerogels for pressure sensing application. Compos Sci Technol. 2021;207:108730.

[6] Zhou S, Apostolopoulou-Kalkavoura V, Tavares da Costa MV, et al. Elastic aerogels of cellulose nanofibers@metal–organic frameworks for thermal insulation and fire retardancy. Nanomicro Lett. 2020;12:9.

[7] Pinto SC, Gonçalves G, Sandoval S, et al. Bacterial cellulose/graphene oxide aerogels with enhanced dimensional and thermal stability. Carbohydr Polym. 2020;230:115598.

[8] Qiu L, Huang B, He Z, et al. Extremely low density and super-compressible graphene cellular materials. Adv Mater. 2017;29:1701553.

[9] Chen Y, Zhang S, Cao S, et al. Roll-to-roll production of metal-organic framework coatings for particulate matter removal. Adv Mater. 2017;29:1606221.

[10] Kitao T, Zhang Y, Kitagawa S, et al. Hybridization of MOFs and polymers. Chem Soc Rev. 2017;46:3108–3133.

[11] Wei H, Li A, Kong D, et al. Polypyrrole/reduced graphene aerogel film for wearable piezoresisitic sensors with high sensing performances. Adv Compos Hybrid Mater. 2021;4:86–95.

[12] He Z, Li X, Wang H, et al. Synergistic regulation of the microstructure for multifunctional graphene aerogels by a dual template method. ACS Appl Mater Interfaces. 2022;14:22544–22553.

[13] Zhang X, Li W, Song P, et al. Double-cross-linking strategy for preparing flexible, robust, and multifunctional polyimide aerogel. Chem Eng J. 2020;381:122784.

[14] Qiu L, Liu JZ, Chang SLY, et al. Biomimetic superelastic graphene-based cellular monoliths. Nat Commun. 2012;3:1241.

[15] Li Y, Chen J, Huang L, et al. Highly compressible macroporous graphene monoliths via an improved hydrothermal process. Adv Mater. 2014;26:4789–4793.

[16] García-Bordejé E, Víctor-Román S, Sanahuja-Parejo O, et al. Control of the microstructure and surface chemistry of graphene aerogels *via* pH and time manipulation by a hydrothermal method. Nanoscale. 2018;10:3526–3539.

[17] Gao H-L, Zhu Y-B, Mao L-B, et al. Super-elastic and fatigue resistant carbon material with lamellar multi-arch microstructure. Nat Commun. 2016;7:12920.

[18] Wang C, Chen X, Wang B, et al. Freeze-casting produces a graphene oxide aerogel with a radial and centrosymmetric structure. ACS Nano. 2018;12:5816–5825.

[19] Zhuo H, Hu Y, Chen Z, et al. Linking renewable cellulose nanocrystal into lightweight and highly elastic carbon aerogel. ACS Sustain Chem Eng. 2020;8:11921–11929.

[20] Zhou Y, Wang S, Li D, et al. Lightweight and recoverable ANF/rGO/PI composite aerogels for broad and high-performance microwave absorption. Compos B Eng. 2021;213:108701.

[21] Hu Y, Zhuo H, Chen Z, et al. Superelastic carbon aerogel with ultrahigh and wide-range linear sensitivity. ACS Appl Mater Interfaces. 2018;10:40641–40650.

[22] Li G, Chu Z, Gong X, et al. A wide-range linear and stable piezoresistive sensor based on methylcellulose-reinforced, lamellar, and wrinkled graphene aerogels. Adv Mater Technol. 2022;7:2101021.

[23] Afroze JD, Tong L, Abden MJ, et al. Hierarchical honeycomb graphene aerogels reinforced by carbon nanotubes with multifunctional mechanical and electrical properties. Carbon N Y. 2021;175:312–321.

[24] Zhang X, Liu P, Duan Y, et al. Graphene/Cellulose nanocrystals hybrid aerogel with tunable mechanical strength and hydrophilicity fabricated by ambient pressure drying technique. RSC Adv. 2017;7:16467–16473.

[25] Qin Y, Peng Q, Ding Y, et al. Lightweight, superelastic, and mechanically flexible graphene/polyimide nanocomposite foam for strain sensor application. ACS Nano. 2015;9:8933–8941.

[26] Xie J, Niu L, Qiao Y, et al. The influence of the drying method on the microstructure and the compression behavior of graphene aerogel. Diam Relat Mater. 2022;121:108772.

[27] Chen Y, Yang L, Xu S, et al. Ultralight aerogel based on molecular-modified poly(*m*-phenylenediamine) crosslinking with polyvinyl alcohol/graphene oxide for flow adsorption. RSC Adv. 2019;9:22950–22956.

[28] Chen X, Liu H, Zheng Y, et al. Highly compressible and robust polyimide/carbon nanotube composite aerogel for high-performance wearable pressure sensor. ACS Appl Mater Interfaces. 2019;11:42594–42606.

[29] Si Y, Wang X, Yan C, et al. Ultralight biomass-derived carbonaceous nanofibrous aerogels with superelasticity and high pressure-sensitivity. Adv Mater. 2016;28:9512–9518.

[30] Yang J, Ye Y, Li X, et al. Flexible, conductive, and highly pressure-sensitive graphene-polyimide foam for pressure sensor application. Compos Sci Technol. 2018;164:187–194.

[31] Sun H, Xu Z, Gao C. Multifunctional, ultra-flyweight, synergistically assembled carbon aerogels. Adv Mater. 2013;25:2554–2560.

[32] Hu H, Zhao Z, Wan W, et al. Ultralight and highly compressible graphene aerogels. Adv Mater. 2013;25:2219–2223.

[33] Kim KH, Tsui MN, Islam MF. Graphene-coated carbon nanotube aerogels remain superelastic while resisting fatigue and creep over −100 to +500 °C. Chem Mater. 2017;29:2748–2755.

[34] Huang Z-M, Liu X-Y, Wu W-G, et al. Highly elastic and conductive graphene/carboxymethylcellulose aerogels for flexible strain-sensing materials. J Mater Sci. 2017;52:12540–12552.

[35] Lin Z, Jiang W, Chen Z, et al. Shape-memory and anisotropic carbon aerogel from biomass and graphene oxide. Molecules. 2021;26:5715.

[36] Peng X, Wu K, Hu Y, et al. A mechanically strong and sensitive CNT/rGO–CNF carbon aerogel for piezoresistive sensors. J Mater Chem A Mater. 2018;6:23550–23559.

[37] Zhao X, Wang W, Wang Z, et al. Flexible PEDOT:PSS/polyimide aerogels with linearly responsive and stable properties for piezoresistive sensor applications. Chem Eng J. 2020;395:125115.

[38] Wu X, Han Y, Zhang X, et al. Large-area compliant, low-cost, and versatile pressure-sensing platform based on microcrack-designed carbon black@polyurethane sponge for human-machine interfacing. Adv Funct Mater. 2016;26:6246–6256.

[39] Wu Y, Liu H, Chen S, et al. Channel crack-designed gold@PU sponge for highly elastic piezoresistive sensor with excellent detectability. ACS Appl Mater Interfaces. 2017;9:20098–20105.

[40] Ge G, Cai Y, Dong Q, et al. A flexible pressure sensor based on rGO/polyaniline wrapped sponge with tunable sensitivity for human motion detection. Nanoscale. 2018;10:10033–10040.

[41] Yao H-B, Ge J, Wang C-F, et al. A flexible and highly pressure-sensitive graphene-polyurethane sponge based on fractured microstructure design. Adv Mater. 2013;25:6692–6698.

[42] Lv B, Chen X, Liu C. A highly sensitive piezoresistive pressure sensor based on graphene oxide/polypyrrole@polyurethane sponge. Sensors. 2020;20:1219.

[43] Long C, Xie X, Fu J, et al. Supercapacitive brophene-graphene aerogel as elastic-electrochemical dielectric layer for sensitive pressure sensors. J Colloid Interface Sci. 2021;601:355–364.

[44] Xu Q, Chang X, Zhu Z, et al. Flexible pressure sensors with high pressure sensitivity and low detection limit using a unique honeycomb-designed polyimide/reduced graphene oxide composite aerogel. RSC Adv. 2021;11:11760–11770.

[45] Luo Q, Zheng H, Hu Y, et al. Carbon nanotube/chitosan-based elastic carbon aerogel for pressure sensing. Ind Eng Chem Res. 2019;58:17768–17775.

[46] Chen Z, Zhuo H, Hu Y, et al. Wood-derived lightweight and elastic carbon aerogel for pressure sensing and energy storage. Adv Funct Mater. 2020;30:1910292.